iMRI

Investigative Magnetic Resonance Imaging

Original Article

Correspondence to:
Ho-Joon Lee, M.D.
Department of Radiology,
Inje University Haeundae Paik
Hospital, 875 Haeun-daero,
Haeundae-gu, Busan 48108,
Korea.
Tel. +82-51-797-0364
Fax. +82-2-2650-5302
E-mail: hojoon.lee@paik.ac.kr

Comparison of 3D Volumetric Subtraction Technique and 2D Dynamic Contrast Enhancement Technique in the Evaluation of Contrast Enhancement for Diagnosing Cushing's Disease

Yae Won Park[1,2], Ha Yan Kim[3], Ho-Joon Lee[2,4], Se Hoon Kim[5], Sun-Ho Kim[6], Sung Soo Ahn[2], Jinna Kim[2], Seung-Koo Lee[2]

[1]Department of Radiology, Ewha Womans University College of Medicine, Seoul, Korea
[2]Department of Radiology and Research Institute of Radiological Science, Yonsei University College of Medicine, Seoul, Korea
[3]Biostatistics Collaboration Unit, Yonsei University College of Medicine, Seoul, Korea
[4]Department of Radiology, Inje University Haeundae Paik Hospital, Busan, Korea
[5]Department of Pathology, Yonsei University College of Medicine, Seoul, Korea
[6]Department of Neurosurgery, Yonsei University College of Medicine, Seoul, Korea

Purpose: The purpose of this study is to compare the performance of the T1 3D subtraction technique and the conventional 2D dynamic contrast enhancement (DCE) technique in diagnosing Cushing's disease.

Materials and Methods: Twelve patients with clinically and biochemically proven Cushing's disease were included in the study. In addition, 23 patients with a Rathke's cleft cyst (RCC) diagnosed on an MRI with normal pituitary hormone levels were included as a control, to prevent non-blinded positive results. Postcontrast T1 3D fast spin echo (FSE) images were acquired after DCE images in 3T MRI and image subtraction of pre- and postcontrast T1 3D FSE images were performed. Inter-observer agreement, interpretation time, multiobserver receiver operating characteristic (ROC), and net benefit analyses were performed to compare 2D DCE and T1 3D subtraction techniques.

Results: Inter-observer agreement for a visual scale of contrast enhancement was poor in DCE (κ = 0.57) and good in T1 3D subtraction images (κ = 0.75). The time taken for determining contrast-enhancement in pituitary lesions was significantly shorter in the T1 3D subtraction images compared to the DCE sequence (P < 0.05). ROC values demonstrated increased reader confidence range with T1 3D subtraction images (95% confidence interval [CI]: 0.94-1.00) compared with DCE (95% CI: 0.70-0.92) (P < 0.01). The net benefit effect of T1 3D subtraction images over DCE was 0.34 (95% CI: 0.12-0.56). For Cushing's disease, both reviewers misclassified one case as a nonenhancing lesion on the DCE images, while no cases were misclassified on T1 3D subtraction images.

Conclusion: The T1 3D subtraction technique shows superior performance for determining the presence of enhancement on pituitary lesions compared with conventional DCE techniques, which may aid in diagnosing Cushing's disease.

Keywords: T1 3D subtraction; 2D dynamic contrast enhancement; Cushing's disease

INTRODUCTION

Cushing's disease, or adrenocorticotrophic hormone (ACTH) secreting pituitary adenoma, comprises 10% of pituitary adenomas, and is responsible for 80-85% of ACTH-dependent Cushing's syndrome (1). The majority of cases are microadenomas that are < 1 cm in size, almost 50% being less than 5 mm, which makes the diagnosis difficult (2). The final diagnosis is often based on magnetic resonance imaging (MRI) and inferior petrosal sinus sampling (3). It is crucial to confirm the pituitary origin of Cushing's syndrome, because the treatment of choice is surgical removal of the lesion (4). However, previous studies have reported that up to 63% of patients have false negative findings on MRI (5-7).

The T1 3D fast spin echo (FSE) MRI has been recently introduced and validated in neuroimaging (8-10), and has shown to provide superior image quality, thinner slices, with less artifacts and partial volume averaging, in the pituitary area, compared to conventional 2D images (11).

The higher SNR attainable and higher field of spatial resolution or spatial resolution with novel sequences has led to improvements in the detection rate (10, 12-14). However, similar or higher false positive rates remain a problem with these conditions (15, 16). In our experience, determination of contrast enhancement in ACTH secreting adenomas may be troublesome due to the partial volume averaging from the frequently small size. volume averaging from the frequently small size. The issue of partial volume averaging was addressed in a study that evaluated the usefulness of sagittal plane dynamic contrast enhancement (DCE) for detection of pituitary adenomas (17). It was reported that the vessel density and area is lower/smaller compared to other pituitary adenomas (18).

Subtraction of an unenhanced T1-weighted sequence from the identical sequence performed after gadolinium administration can be helpful for determination of contrast enhancement, especially when the lesions are hyposignal or hypersignal compared to the surrounding structures on T1 weighted images (19-22). Subtraction of an unenhanced T1-weighted sequence was shown to be superior in the evaluation of signal intensity differences compared to conventional side-to-side review, given that the images are well-registered, which improves quality of the subtraction map and diminishes undesired artifacts (23).

It is noteworthy that visual assessment is vulnerable to optical illusions. Also, comparison of the region of interest based on measurements between precontrast and postcontrast images on a picture archiving and communication system may be misleading due to platform based scaling in certain situations (24).

We hypothesized that the assessment of T1 3D subtraction method can determine contrast enhancement in pituitary lesions with increased accuracy, better confidence, and a shorter review time, compared to the conventional DCE technique.

MATERIALS AND METHODS

Subjects

Patient consent was waived for this retrospective study. Between May 2015 and November 2016, 12 patients with clinically and biochemically proven Cushing's disease underwent 3.0 T MRIs in our hospital. The sample was comprised of 10 women, 2 men; mean age, 37 years with an age range of 16-66 years. All of the patients underwent inferior petrosal sinus sampling, and the petrosal/peripheral ACTH ratio was > 2 at baseline, and > 3 at 5 minutes after 10 μg of desmopressin was injected intravenously. In addition, 23 patients with a Rathke's cleft cyst (RCC) diagnosed on an MRI with normal pituitary hormone levels were included. This group was comprised of 20 women, 3 men; mean age, 40.3 years with an age range of 22-81 years as a control group, to prevent non-blinded positive results. The imaging diagnosis of RCC was determined by consensus.

Among the 12 Cushing's disease cases, 9 cases were surgically confirmed. One patient did not receive surgery due to old age, and 2 patients underwent surgery, but an immunohistochemical study could not be performed due to loss of the small tumor tissue during a frozen biopsy and serial section

Magnetic Resonance Imaging

Patients were scanned on 3.0 Tesla MRI units (Discovery MR750/750w; GE Healthcare, Milwaukee, WI, USA), with a 32 channel head coil. After a pre-contrast T1 3D FSE scan, DCE images were obtained immediately after the bolus injection of 0.1 mmol/kg of Gadolinium contrast agent (Dotarem; Guerbet, SA, France) that was at a rate of 2 ml/s via an antecubital venous access. Postcontrast T1 3D FSE images were acquired after DCE images, with a 3D fast spoiled gradient echo (FSPGR, acquisition time: 3:29) sequence in between. Detailed MR parameters for conventional DCE imaging and T1 3D FSE are summarized

iMRI

3D Subtraction and 2D DCE in Cushing's Disease | Yae Won Park, et al.

in Table 1. In some cases of Cushing's disease (n = 6), conventional 2D DCE acquired at another institute was reviewed instead, because an alternative dynamic technique was applied for these cases at our institute. Only images taken within a period of three months were included, and the image quality and parameters were acceptable for visual assessment and similar to those of our imaging protocol.

Image Subtraction

Precontrast T1 3D FSE images were registered to postcontrast T1 3D FSE images by using rigid transformation with least-squares as cost functions (25). The registered precontrast T1 3D FSE images were subtracted from postcontrast T1 3D FSE and stored for visual analysis. The above steps were performed with the Medical Processing, Analysis, and Visualization software package version 7.3.0 (National Institutes of Health; mipav.cit.nih.gov).

Image Assessment

The DCE sequences and T1 3D subtraction images were reviewed in random order. Two neuroradiologists with 1 and 3 years of experience with pituitary MRIs, reviewed the sequences independently, and were blind to the clinical history and the diagnosis. The reviewers recorded the interpretation time taken to draw a conclusion (in seconds). Visual scoring was performed by a three-point scale of contrast enhancement (0: no contrast enhancement, 1: suspicious contrast enhancement, 2: definite contrast enhancement) on DCE images in the first session. To minimize the recall bias, the second session was done a week later for T1 3D subtraction images in the same way. On T1 3D subtraction images, contrast enhancement of the pituitary lesion was defined as a higher signal on the visual assessment compared to the subtracted temporal white matter. During both sessions, contrast-enhanced T1 3D fast spoiled gradient echo (FSPGR) sequence was used as a reference for lesion localization.

Statistical Analysis

Inter-observer agreement for visual conspicuity was analyzed using weighted Cohen kappa coefficient: κ values > 0.81, were in the range of 0.61-0.80, and < 0.60 were considered to reflect excellent, good, and poor agreement, respectively. A Mann-Whitney test was performed to compare the interpretation time of each sequences. The receiver operating characteristic (ROC) for multireader-multicase (MRMC) analysis was performed with the Dorfman-Berbaum-Metz approach by using readers as

fixed variables and cases as random variables (26, 27). All P-values < 0.05 were considered statistically significant. A net benefit effect measure that combines sensitivity and specificity, adjusted for prevalence was calculated, and bootstrapped data was used to derive the confidence interval (CI). The net benefit effect is defined as the difference in sensitivity with use of T1 3D subtraction technique plus the difference in specificity with use of T1 3D subtraction technique, with the difference in specificity weighted by two factors. Those two factors being: (a) a weighting value, defined as the relative increased in value (i.e., benefit, cost, or utility) of an additional correctly identified patient with a true-positive diagnosis compared with the reduction in value of an additional patient with a false-positive diagnosis; and (b) an adjustment for prevalence (i.e., proportion of true-positive diagnoses) (28). A significant improvement with T1 3D subtraction technique was defined as a positive net-effect measure whose 95% CI did not include zero. Statistical analysis was performed using SPSS Statistics 23.0 (IBM, Armonk, NY, USA), MRMC analysis was performed with SAS (version 9.4, SAS Inc., Cary, NC, USA), OR-DBM MRMC 2.5 software; University of Iowa, Iowa City, IA), and R statistical software R (version 3.3.1; R Foundation for Statistical Computing, Vienna, Austria).

RESULTS

Inter-observer agreement for visual scale of contrast enhancement was poor in DCE (κ = 0.57) and good in

Table 1. Imaging Parameters for the Conventional Dynamic Enhancement and T1 3D Fast Spin Echo Sequences

	Dynamic contrast enhancement	T1 3D fast spin echo
Field of view (mm)	180	180
Matrix size	384 × 256	384 × 256
Slice thickness/spacing (mm)	2/3	1/0.5
TR/TE (ms)	380 or 325/9.6 or 10.1	530/16 or 17
Flip angle	111	Variable
Echo train length	3	24
Number of excitations	1	2
Scan time (minutes: seconds)	2:36 (31seconds/ phase)	3:16

TE = echo time; TR = repetition time

T1 3D subtraction images (κ = 0.75). The time taken for determining presence of contrast-enhancement in pituitary lesions was significantly shorter in the T1 3D subtraction images compared to the DCE sequence in the whole group (8.1 ± 5.2 seconds and 17.9 ± 12.0 seconds for T1 3D subtraction technique and DCE, respectively, P < 0.05) (Table 2).

Mean ROC values demonstrated increased reader confidence range with subtraction images (0.975, 95% CI: 0.94-1.00) compared with DCE (0.799, 95% CI: 0.70-0.92) (P < 0.01). Net benefit effect of subtraction images over DCE was 0.34 (95% CI: 0.12-0.56), which is also in concordance with the above results.

For Cushing's disease, both reviewers misclassified one case as a non-enhancing lesion on DCE images, while no cases were misclassified on T1 3D subtraction images by either reviewer. For RCC, four cases by reviewer 1 and five cases by reviewer 2 were misclassified as an enhancing lesion on DCE images, while only one case was misclassified as an enhancing lesion by reviewer 2 on T1 3D subtraction images (Table 3).

Figures 1 and 2 show examples of Cushing's disease and RCC cases misclassified with DCE and correctly classified by T1 3D subtraction images.

DISCUSSION

Our study shows that the T1 3D subtraction technique reduces inter-observer variability and increases reader confidence, requires significantly less interpretation time, and increases the accuracy of assessing contrast enhancement compared to the conventional 2D dynamic scan.

Image subtraction could be applied to a routine MRI, using a variety of commercially or non-commercially available workstations or software products. Image subtraction can also be integrated into the clinical workflow effortlessly, since only minimal processing time for registration and subtraction is required. In our study, we included RCC patients as a control because including only Cushing's disease patients in diagnosing the presence of contrast-enhancing lesions may lead to false positive results. The results are noteworthy, because the conventional 2D dynamic in this study shows a high proportion of misclassification and variability in both Cushing's disease and RCC.

To the best of our knowledge, there has been no previous study to compare the pre-postcontrast subtraction image and conventional dynamic study in the evaluation of Cushing's disease. ACTH-secreting adenomas have the tendency to be microadenomas that are intrasellar in location (29, 30). The success of surgery in Cushing's disease largely relies on precisely locating the tumor within the sella turcica (31). The accuracy of the conventional dynamic MRI in diagnosing Cushing's disease is suboptimal, only confirming approximately 50-70% of Cushing's disease cases (6, 7, 31, 32). Previous studies have shown that dynamic spin echo imaging acquired 30 to 90 seconds after contrast injection demonstrated the best contrast for microadenomas (33, 34), and the maximal contrast was obtained within a 2 minute window after contrast injection (35). The partial volume effect between micro-lesions and surrounding tissues can lead to pseudoenhancement in pituitary gland lesions and there is no evidence on how long the dynamic scan should be to

Table 2. Interpretation Time (second) Taken for Determination of Contrast Enhancement

	DCE	T1 3D subtraction	P value
Cushing + RCC (n = 35)	17.9 ± 12.0	8.1 ± 5.2	< 0.001
Cushing (n = 12)	23.5 ± 15.2	9.5 ± 6.7	< 0.001
RCC (n = 23)	15.0 ± 8.7	7.4 ± 4.2	< 0.001

DCE = dynamic contrast enhancement; RCC = Rathke's cleft cyst

Table 3. Interpretation Results for Diagnosis of Cushing Disease and RCC on DCE and Subtraction Images

		Cushing (n = 12)			RCC (n = 23)		
		CE	Suspicious	NCE	CE	Suspicious	NCE
Reviewer 1	DCE	9 (75)	2 (16.7)	1 (8.3)	4 (17.4)	8 (34.8)	11 (47.8)
	T1 3D subtraction	12 (100)	0 (0)	0 (0)	0 (0)	1 (4.3)	22 (95.7)
Reviewer 2	DCE	8 (66.7)	3 (25.0)	1 (8.3)	5 (21.7)	5 (21.7)	13 (56.6)
	T1 3D subtraction	8 (66.7)	4 (33.3)	0 (0)	1 (4.4)	3 (13.0)	19 (82.6)

Data are presented as number of patients (%).
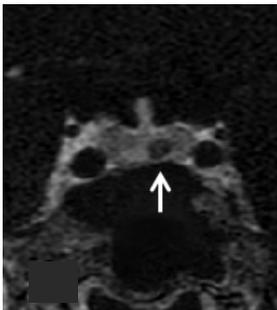CE = contrast enhancement; DCE = dynamic contrast enhancement; NCE = no contrast enhancement; RCC = Rathke's cleft cyst

iMRI

3D Subtraction and 2D DCE in Cushing's Disease | Yae Won Park, et al.

detect contrast enhancement. The 3D FSE with a variable flip angle technique enables thin slice imaging without exceeding specific absorption rate (SAR) limits (36). The 3D FSE can potentially minimize the partial volume effect between micro-lesions and surrounding tissues, which may contribute to the detection of pituitary micro-lesions
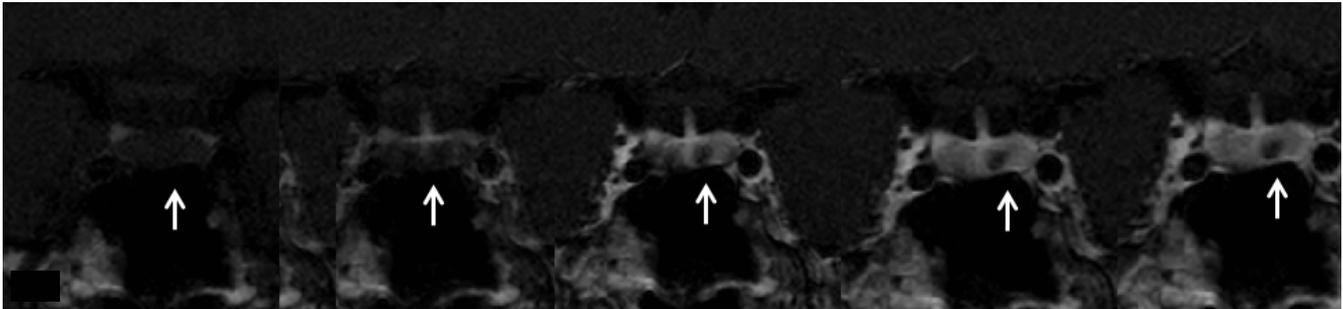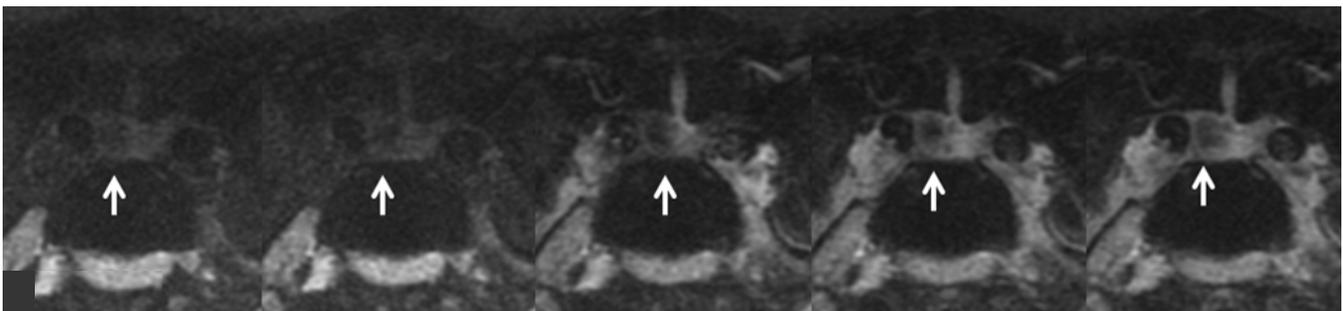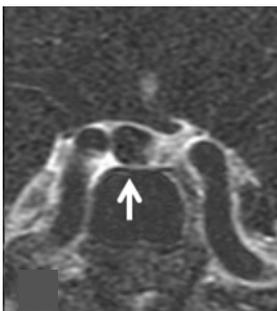

a

b

Fig. 1. Images of a 37-year-old female patient diagnosed with Cushing disease. On conventional dynamic contrast enhanced images (a), both reviewers recorded the visual scale as 1 (suspicious enhancement) (arrows). On subtraction image (b), there is definite contrast enhancement of the lesion, which was defined as having a higher value compared to the subtracted temporal white matter. Both reviewers recorded the visual scale as 2 (definite contrast enhancement) (arrow).

a

b

Fig. 2. Images of a 32-year-old female patient diagnosed with Rathke's cleft cyst. On conventional dynamic images (a), reviewer 1 recorded the visual scale as 1 (suspicious contrast enhancement) and reviewer 2 recorded the visual scale as 2 (definite contrast enhancement) (arrows). On subtraction image (b), there is no contrast enhancement of the lesion and both reviewers recorded the visual scales as 0 (no contrast enhancement) (arrow).

(37). Furthermore, the subtraction technique used in our study may be advantageous for detection of adenomas with slower enhancement, since the postcontrast T1 3D FSE images were acquired more slowly at a delayed phase after contrast enhancement. However, even with the combination of T1 3D subtraction technique, the presence of contrast enhancement still resulted in misclassification in some cases. These errors may be further improved by the application of more advanced imaging techniques such as 3D CAIPIRINHA (controlled aliasing in parallel imaging results in higher acceleration) (38), compressed sensing (39), or reduced field-of-view imaging (40, 41), which can provide higher spatial resolution without increasing scan time.

In a recent review, it was recommended (42), that higher resolution DCE scans (field of view 12-14 cm, matrix size 256 × 192, slice thickness 1-1.5 mm) should be used when Cushing's disease is suspected. Advanced techniques that enable volumetric dynamic imaging with thin slices are becoming more available (43, 35). These approaches may prove to be alternate approaches that can minimize partial volume averaging, and decrease ambiguity in determining contrast enhancement.

There are several limitations in our study. First, only the presence of contrast enhancement with conventional DCE and T1 3D subtraction images were evaluated for the pituitary lesion, which may not reflect the practical situation. In routine practice, T1 weighted and T2 weighted images are also included in the evaluation of a pituitary lesion, from which additional information can be drawn. Second, features that affect diagnosis such as location of the lesion (42), could not be blinded in our study although the reviewers focused on contrast enhancement as much as possible, this can be a potential source of bias. Third, our study design is a retrospective study with a case-control design. Fourth, a substantial proportion of our Cushing's disease patients had performed DCE at another institution, which may affect the interpretation results due to different MRI protocols.

In conclusion, the T1 3D subtraction technique shows superior performance for determining the presence of enhancement on pituitary lesions compared with the conventional DCE technique, which may aid in diagnosing Cushing's disease.

REFERENCES

1. Juszczak A, Grossman A. The management of Cushing's disease - from investigation to treatment. Endokrynol Pol 2013;64:166-174
2. Newell-Price J, Trainer P, Besser M, Grossman A. The diagnosis and differential diagnosis of Cushing's syndrome and pseudo-Cushing's states. Endocr Rev 1998;19:647-672
3. Potts MB, Shah JK, Molinaro AM, et al. Cavernous and inferior petrosal sinus sampling and dynamic magnetic resonance imaging in the preoperative evaluation of Cushing's disease. J Neurooncol 2014;116:593-600
4. Witek P, Zielinski G. Predictive value of preoperative magnetic resonance imaging of the pituitary for surgical cure in Cushing's disease. Turk Neurosurg 2012;22:747-752
5. Davis WL, Lee JN, King BD, Harnsberger HR. Dynamic contrast-enhanced MR imaging of the pituitary gland with fast spin-echo technique. J Magn Reson Imaging 1994;4:509-511
6. Bartynski WS, Lin L. Dynamic and conventional spin-echo MR of pituitary microlesions. AJNR Am J Neuroradiol 1997;18:965-972
7. Ludecke DK, Flitsch J, Knappe UJ, Saeger W. Cushing's disease: a surgical view. J Neurooncol 2001;54:151-166
8. Busse RF, Brau AC, Vu A, et al. Effects of refocusing flip angle modulation and view ordering in 3D fast spin echo. Magn Reson Med 2008;60:640-649
9. Kato Y, Higano S, Tamura H, et al. Usefulness of contrast-enhanced T1-weighted sampling perfection with application-optimized contrasts by using different flip angle evolutions in detection of small brain metastasis at 3T MR imaging: comparison with magnetization-prepared rapid acquisition of gradient echo imaging. AJNR Am J Neuroradiol 2009;30:923-929
10. Kitajima M, Hirai T, Shigematsu Y, et al. Comparison of 3D FLAIR, 2D FLAIR, and 2D T2-weighted MR imaging of brain stem anatomy. AJNR Am J Neuroradiol 2012;33:922-927
11. Lien RJ, Corcuera-Solano I, Pawha PS, Naidich TP, Tanenbaum LN. Three-tesla imaging of the pituitary and parasellar region: T1-weighted 3-dimensional fast spin echo cube outperforms conventional 2-dimensional magnetic resonance imaging. J Comput Assist Tomogr 2015;39:329-333
12. Wolfsberger S, Ba-Ssalamah A, Pinker K, et al. Application of three-tesla magnetic resonance imaging for diagnosis and surgery of sellar lesions. J Neurosurg 2004;100:278-286
13. Pinker K, Ba-Ssalamah A, Wolfsberger S, Mlynarik V, Knosp E, Trattnig S. The value of high-field MRI (3T) in the

iMRI

3D Subtraction and 2D DCE in Cushing's Disease | Yae Won Park, et al.

assessment of sellar lesions. Eur J Radiol 2005;54:327-334

14. de Rotte AA, Groenewegen A, Rutgers DR, et al. High resolution pituitary gland MRI at 7.0 tesla: a clinical evaluation in Cushing's disease. Eur Radiol 2016;26:271-277

15. Patronas N, Bulakbasi N, Stratakis CA, et al. Spoiled gradient recalled acquisition in the steady state technique is superior to conventional postcontrast spin echo technique for magnetic resonance imaging detection of adrenocorticotropin-secreting pituitary tumors. J Clin Endocrinol Metab 2003;88:1565-1569

16. Stobo DB, Lindsay RS, Connell JM, Dunn L, Forbes KP. Initial experience of 3 tesla versus conventional field strength magnetic resonance imaging of small functioning pituitary tumours. Clin Endocrinol (Oxf) 2011;75:673-677

17. Lee HB, Kim ST, Kim HJ, et al. Usefulness of the dynamic gadolinium-enhanced magnetic resonance imaging with simultaneous acquisition of coronal and sagittal planes for detection of pituitary microadenomas. Eur Radiol 2012;22:514-518

18. Takano S, Akutsu H, Hara T, Yamamoto T, Matsumura A. Correlations of vascular architecture and angiogenesis with pituitary adenoma histotype. Int J Endocrinol 2014;2014:989574

19. Secil M, Obuz F, Altay C, et al. The role of dynamic subtraction MRI in detection of hepatocellular carcinoma. Diagn Interv Radiol 2008;14:200-204

20. Yu JS, Kim YH, Rofsky NM. Dynamic subtraction magnetic resonance imaging of cirrhotic liver: assessment of high signal intensity lesions on nonenhanced T1-weighted images. J Comput Assist Tomogr 2005;29:51-58

21. Tay KL, Yang JL, Phal PM, Lim BG, Pascoe DM, Stella DL. Assessing signal intensity change on well-registered images: comparing subtraction, color-encoded subtraction, and parallel display formats. Radiology 2011;260:400-407

22. Yu JS, Rofsky NM. Dynamic subtraction MR imaging of the liver: advantages and pitfalls. AJR Am J Roentgenol 2003;180:1351-1357

23. Sundarakumar DK, Wilson GJ, Osman SF, Zaidi SF, Maki JH. Evaluation of image registration in subtracted 3D dynamic contrast-enhanced MRI of treated hepatocellular carcinoma. AJR Am J Roentgenol 2015;204:287-296

24. Chenevert TL, Malyarenko DI, Newitt D, et al. Errors in quantitative image analysis due to platform-dependent image scaling. Transl Oncol 2014;7:65-71

25. Feldmar J, Ayache N. Rigid, affine and locally affine registation of free-form surfaces. Int J Comput Vis 1996;18:99-119

26. Harrigan CJ, Peters DC, Gibson CM, et al. Hypertrophic cardiomyopathy: quantification of late gadolinium enhancement with contrast-enhanced cardiovascular MR imaging. Radiology 2011;258:128-133

27. Saade C, El-Merhi F, Mayat A, Brennan PC, Yousem D. Comparison of standard and quadruple-phase contrast material injection for artifacts, image quality, and radiation dose in the evaluation of head and neck cancer metastases. Radiology 2016;279:571-577

28. Halligan S, Altman DG, Mallett S. Disadvantages of using the area under the receiver operating characteristic curve to assess imaging tests: a discussion and proposal for an alternative approach. Eur Radiol 2015;25:932-939

29. Jagannathan J, Dumont A, Jane JA Jr. Diagnosis and management of pediatric sellar lesions. In Laws ER Jr, Sheehan JP, eds. Pituitary surgery - a modern approach. Front Horm Res. Basel: Karger, 2006:83-104

30. Jagannathan J, Dumont AS, Jane JA Jr, Laws ER Jr. Pediatric sellar tumors: diagnostic procedures and management. Neurosurg Focus 2005;18:E6

31. Ikeda H, Abe T, Watanabe K. Usefulness of composite methionine-positron emission tomography/3.0-tesla magnetic resonance imaging to detect the localization and extent of early-stage Cushing adenoma. J Neurosurg 2010;112:750-755

32. Colao A, Boscaro M, Ferone D, Casanueva FF. Managing Cushing's disease: the state of the art. Endocrine 2014;47:9-20

33. Elster AD. High-resolution, dynamic pituitary MR imaging: standard of care or academic pastime? AJR Am J Roentgenol 1994;163:680-682

34. Kucharczyk W, Bishop JE, Plewes DB, Keller MA, George S. Detection of pituitary microadenomas: comparison of dynamic keyhole fast spin-echo, unenhanced, and conventional contrast-enhanced MR imaging. AJR Am J Roentgenol 1994;163:671-679

35. Rossi Espagnet MC, Bangiyev L, Haber M, et al. High-Resolution DCE-MRI of the pituitary gland using radial k-space acquisition with compressed sensing reconstruction. AJNR Am J Neuroradiol 2015;36:1444-1449

36. Kartal MG, Algin O. Evaluation of hydrocephalus and other cerebrospinal fluid disorders with MRI: An update. Insights Imaging 2014;5:531-541

37. Wang J, Wu Y, Yao Z, Yang Z. Assessment of pituitary micro-lesions using 3D sampling perfection with application-optimized contrasts using different flip-angle evolutions. Neuroradiology 2014;56:1047-1053

38. Fritz J, Fritz B, Thawait GG, Meyer H, Gilson WD, Raithel E. Three-dimensional CAIPIRINHA SPACE TSE for 5-minute high-resolution MRI of the knee. Invest Radiol 2016;51:609-617

iMRI

39. Fritz J, Ahlawat S, Demehri S, et al. Compressed sensing SEMAC: 8-fold accelerated high resolution metal artifact reduction MRI of cobalt-chromium knee arthroplasty implants. Invest Radiol 2016;51:666-676

40. Schulze M, Reimann K, Seeger A, Klose U, Ernemann U, Hauser TK. Improvement in imaging common temporal bone pathologies at 3 T MRI: small structures benefit from a small field of view. Clin Radiol 2017;72:267 e261-267 e212

41. Seeger A, Schulze M, Schuettauf F, Klose U, Ernemann U, Hauser TK. Feasibility and evaluation of dual-source transmit 3D imaging of the orbits: comparison to high-resolution conventional MRI at 3T. Eur J Radiol 2015;84:1150-1158

42. Vitale G, Tortora F, Baldelli R, et al. Pituitary magnetic resonance imaging in Cushing's disease. Endocrine 2017;55:691-696

43. Fushimi Y, Okada T, Kanagaki M, et al. 3D dynamic pituitary MR imaging with CAIPIRINHA: initial experience and comparison with 2D dynamic MR imaging. Eur J Radiol 2014;83:1900-1906